DESIGN OF A SPARSE PLANAR ARRAY FOR OPTIMIZED 3D MEDICAL ULTRASOUND IMAGING

Claudia Sciallero[1] *and Andrea Trucco*[1,2]

[1]Dept. of Electrical, Electronic, Telecommunications Engineering, and Naval Architecture (DITEN)
University of Genoa, Genova, Italy
[2]Pattern Analysis & Computer Vision, Istituto Italiano di Tecnologia (IIT), Genova, Italy

ABSTRACT

Two-dimensional apertures provide fully electronic scanning for 3D medical ultrasound imaging. The design of planar arrays with a limited number of active elements yielding real-time 3D high-quality imaging, for all beam scanning orientations, is one of the current challenges. In this paper, an innovative transmission/reception solution, that involves a compact fully sampled 256-element array as transmitter and an optimized 256-element sparse array as receiver, able to fulfill all the previous requirements, is proposed. The sparse array is made up of a thinned version of the transmitter dense array (i.e., a proper subset of elements is used both to transmit and receive) surrounded by an annular sparse off-the-grid array. Both the positions and the weights of the sparse array are jointly optimized by minimizing a novel cost function by means of simulated annealing algorithm. The proposed solution is well-suited for real-time 3D imaging over 360° of azimuth and ±40° of inclination.

Index Terms— 3D medical ultrasound imaging, planar array, sparse array, stochastic optimization, ultrasound signal processing

1. INTRODUCTION

A transducer array formed of multiple elements in two dimensions enables to scan beams over a three dimensional volume, providing a fully electronic scanning for 3D medical ultrasound imaging. When a 2D array scans in any direction in a 3D volume, it is desirable that high-quality imaging can be achieved for all beam scanning orientations. To prevent grating lobes (i.e., aliasing effects due to spatial under-sampling) and improve steering capabilities, the maximum spacing between the array element centers of nearest neighbor rows in any direction should not exceed one-half wavelength (λ/2). When a fine lateral resolution is requested, the array should have a wide spatial extension and consequently the number of active elements drastically increases under λ/2-condition. The use of unequally spaced arrays (i.e., aperiodic arrays) is a method to reduce the number of active elements and to limit the cost of 2D arrays, because an acquisition channel is associated with each array element. A fully sampled array is thinned by periodically or randomly removing a fraction of the original set of elements, thus obtaining a sparse array [1,2]. Otherwise, when the element positioning does not follow any regular grid disposition we are dealing with random and non-grid sparse arrays [3,4]. The main drawback of sparse arrays is an increase of the side lobe levels, therefore an optimization of the element position and/or element weight is necessary [1-4]. Generally, the synthesis of sparse 2D arrays is based exclusively on the optimization of the one-way response, i.e., one-way beam pattern (BP). The same optimized array is supposed to be used as transmitter and receiver. The acoustic beam characteristics are improved. On the other side, when a large planar array is considered (characterized by a narrow main lobe), a high amount of beams has to be acquired both in transmission and reception to cover the 3D volume, especially when a wide range of steering angles is considered. An effective real-time acquisition can be compromised. The latest problem is scarcely addressed in literature. Moreover, although the BP of a 2D array is a 3D surface, generally the optimization procedure is not valid over 360° of azimuth and only the BP profile along one or two axes are evaluated to define the array performance.

In this paper, an innovative transmission/reception solution well-suited for real-time low-cost 3D high-quality imaging, for all beam scanning orientations, with a view to real and concrete applications is presented. A compact circular fully sampled 256-element array is used as transmitter to generate a homogeneous and quite wide beam profile. An optimized 256-element sparse array made up of a thinned version of the transmitter dense array (i.e., a proper subset of elements is used both to transmit and receive) surrounded by an annular sparse off-the-grid array is used as receiver. Both the positions and the weights of the sparse array are jointly optimized by minimizing a novel cost function by means of the simulated annealing algorithm [5]. The optimization procedure is valid for the 3D BP. The obtained 3D BP should be similar to a desired 3D BP. In this case, the characteristics of the desired BP are fixed in order to optimize the overall BP (i.e., the two-way 3D BP, where the transmitter is a

This work has been supported by the Italian Ministry of Education, University and Research (PRIN 2010-2011).

978-0-9928626-3-3/15/$31.00 ©2015 IEEE

dense array and the receiver is a larger optimized sparse array) in terms of main lobe width and side lobe levels. The favorable aspects of the proposed solution are: i) two different arrays in one are considered; ii) a limited number of active elements are considered (low-cost arrays); iii) the relative low spatial resolution of the transmitter array is recovered by the larger receiver array; iv) the number of beams required to scan the whole 3D volume is reduced (a lower number of beams is used in transmission); v) the optimization process is extended over 360° of azimuth, producing a quite uniform response for all axes orientations; vi) uniform performance over a wide range of steering angles is guaranteed.

2. TRANSMITTER AND RECEIVER ARRAY LAYOUTS

2.1. Dense array

A compact circular fully sampled 256-element array is used as transmitter. The 2D array is formed of a plurality of elements which are closely packed in a hexagonal grid pattern. A maximum pitch (i.e., spacing between the array element centers of nearest neighbor rows) of $\lambda/2$ is considered. The placement of the element centers is depicted in Fig. 1.

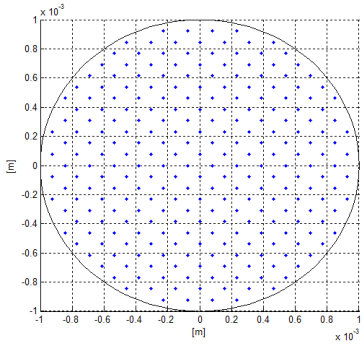

Fig. 1. Layout of the transmitter 2D dense array: element center positioning.

2.2. Sparse array

The receiver planar array is composed of two subparts. The central footprint is equal to the transmitter array footprint because a subset of elements that are used to transmit are opportunely activated also during the reception phase. In this case, a sparse array derived from a regular grid is obtained. The central part of the array is surrounded by an annular sparse off-the-grid array. The maximum radius of the circular array is equivalent to the radius of a theoretical dense 256-element array with inter element spacing of 1.5λ. The element positioning of the second subpart of the receiver array does not following any particular order. Non-grid sparse array techniques are generally applied to reduce the grating and side lobe levels. Since two different sparse-array techniques are used to generate the receiver array, this non-conventional array layout will be referred to as "hybrid sparse array". The positions and weights of the elements of the hybrid sparse array will be optimized. To reduce the optimization computational load (i.e., to reduce the number of elements that has to be perturbed by the optimization algorithm) and to obtain a more uniform 3D beam profile, we have introduced some layout symmetries for the design of the receiver array. The 4-quadrant symmetry of the central array (i.e., equivalent to the transmitter array) can be exploited: the active elements of the other quadrants are derived through an opportune rotation of the configuration selected for the first quadrant. On the other hand, in the annular sparse off-the-grid array a semi-quadrant symmetry is chosen. An example of a possible configuration (random non-optimized configuration) of the receiver hybrid sparse array is shown in Fig. 2.

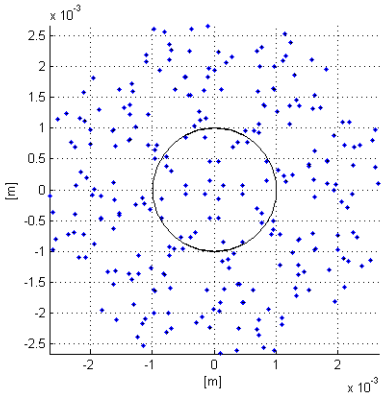

Fig. 2. Example of the receiver 2D hybrid sparse array layout (element center positioning). The circle delimited the thinned version of the transmitter dense array (Fig. 1).

3. COST FUNCTION

Under wide-band conditions, a redefinition of the BP is needed because the conventional formulation (for narrow-band condition) is not valid any more. When a plane wave reaches the array at a given incidence angle, the signals received by the sensors can be modeled as a replica of the transmitted pulse, adequately delayed in accordance with the incident angle and the positions of the array elements. The value of the BP for a pair of beam direction vectors, i.e., $u = sin\theta \cdot cos\varphi$ and $v = sin\theta \cdot sin\varphi$ where θ is the elevation and φ the azimuth angles, respectively, can be considered as the maximum of the beam signal over time.
To define the cost function, a preliminary analysis of the results obtained when the dense array and a non-optimized hybrid sparse array are used has to be performed. It is to be noticed that, as a consequence of the adopted transmission/reception solution, the area irradiated by each transmitted beam has to be covered by multiple-beams during the reception phase. A possible transmission/reception beam scheme is reported in Fig. 3. The circles represent the section of the main lobe at -3 dB (the diameter is the main lobe width). In this case, for each transmitted beam, 9 beams has to be generated in reception (e.g., transmitter main lobe width = 6.4° and receiver main lobe width = 2.4°). This means that the steering direction used in reception can be different from the steering direction used in transmission. This fact can cause the rise of undesired side lobes very close to the main lobe. An example is reported

in Fig. 4. The two-way 3D BP is shown by assuming a broadside transmission and a steering of θ = 2° and φ = 0° in reception.

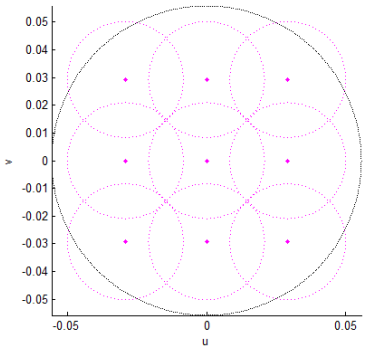

Fig. 3. Example of the transmission/reception beam scheme. The circles represent the main lobe width at -3 dB: one beam for transmission (dense array) and 9 beams for reception (larger hybrid sparse array).

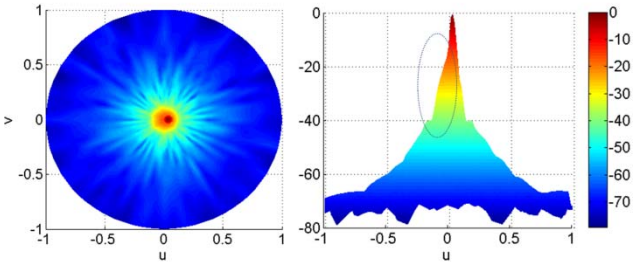

Fig. 4. Two-way 3D BP. Appearance of undesired side lobes very close to the main lobe when the transmission and reception steering does not coincide. Colorbar shows the dB values.

The cost function $f(\boldsymbol{W},\boldsymbol{P})$ should be able to provide a measure of the difference between the desired BP (BP_d) and the current one, obtained by using the actual positions $\boldsymbol{P}$ and the actual weights $\boldsymbol{W}$. The number of active elements and the spatial aperture are fixed. We want to guarantee a good image resolution, low side lobe levels, especially when transmission and reception steering does not coincide, and a general validity over 360° of azimuth. Toward this end, considering the dependency of the BP from θ and φ, $BP(\theta,\varphi)$, the following formulation can be adopted:

$$f(\boldsymbol{W},\boldsymbol{P}) = \left[{}^{1}\!/_{Q} \sum_{\varphi[0°,90°]} k_0 \left(BP(\theta_0,\varphi) - BP_d(\theta_0,\varphi)\right)_+ + k_1 \int_{\theta_1}^{\theta_2} \left(BP(\theta,\varphi) - BP_d(\theta,\varphi)\right)_+ d\theta + k_2 \int_{\theta_2}^{\theta_3} \left(BP(\theta,\varphi) - BP_d(\theta,\varphi)\right)_+ d\theta \right]^2 \quad (1)$$

where Q is the number of discretization along the azimuth angle (φ), ranging between 0 degree and 90 degree due to the symmetry assumptions, k_0, k_1 and k_2 are three constants denoting the relative importance assigned to the BP difference. $BP(\theta,\varphi)$ and $BP_d(\theta,\varphi)$ are calculated in linear scale and normalized (only for $\theta \geq 0°$, as a consequence of the symmetry assumptions). The first term is introduced to limit the BP main lobe (i.e., the lateral resolution): for every discrete value of the azimuth angle, the 2D BP calculated in θ_0 (θ_0 is set on the base of the desired resolution) is forced to a value (generally equal to -3 dB in the logarithmic scale). Then, two different regions of the BP are individuated ranging between θ_1 and θ_2 in the first case and between θ_2 and θ_3 in the second one. The first region that is closer to the main lobe will be forced to very low levels to reduce the side lobes, while for the second one the constraint will be relaxed. Finally, $(BP(\theta,\varphi) - BP_d(\theta,\varphi))_+$ means that only the values that fulfill the relation $BP(\theta,\varphi) > BP_d(\theta,\varphi)$ are taken into account to compute the cost function.

4. OPTIMIZATION DETAILS

During the minimization process, the array elements are divided into two sets: the set of elements that lays in the central part of the array (same footprint of the transmitter array) and the set of elements that lays in the external annular array. In this study, the number of elements positioned in the two different subparts is fixed before the optimization process starts and does not change during the algorithm iterations. Two different initial temperatures are chosen: one for the element position optimization, while the second controls the element weights. The temperature is a parameter of the simulated annealing (SA) [5] that, as the iteration go on, is gradually lowered following a given scheduling (typically the reciprocal of the logarithm of the number of iterations), until the configuration freezes in a final state. The temperature plays the important role of making it possible to escape from local minima. With two different initial temperatures it is possible for example to freeze before the end of the iterations the elements positions and keep changing the element weights.

When an iteration starts, one chooses an element randomly. If the chosen element is in the central part of the array, one can move it according to the regular grid. If the chosen element is in the annular external array, the element can be moved in any position in the annular array footprint. On the base of the element dimension, the center of the element is chosen in order to avoid any element overlapping. On the basis of the temperature (position temperature, T_P), such state transition can be accepted or not. After the positioning procedure, one can perturb the weight coefficient of the chosen element. The coefficient values are included in an a priori set range $[w_{min}, w_{max}]$. Again, on the basis of the temperature (weight temperature, T_W), such state transition can be accepted or not. The number of iterations is increased every time all the elements have been perturbed one (both position and weight). One can perform a number of iterations that is large enough to ensure that a block state will be reached.

5. RESULTS

The BP is evaluated under the following conditions: 6-cycle acoustic pulse with a central frequency of 7 MHz shaped by Gaussian envelope and characterized by a fractional bandwidth of 50%. The focus depth is fixed at 2.5 cm. The optimization algorithm parameters are set as follows: $k_0 = 900$, $k_1 = 200$, $k_2 = 1$, $T_P = 400$, $T_W = 100$, $w_{min} = 0.25$, $w_{max} = 1.75$, $\varphi = [0°, 10°, 20°, 30°, 40°, 45°, 50°, 60°, 70°, 80°]$ and the number of iterations is equal to 800. The chosen parameters are: $\theta_0 = 1.25°$ (i.e., semi-width of the main lobe that corresponds to a lateral resolution of 1 mm at a depth of 2.5 cm), $\theta_1 = 4°$, $\theta_2 = 30°$ and $\theta_3 = 90°$. In the first region, the desired BP is fixed to -40 dB, while in the second region to -25 dB. 32 elements are positioned in the central subpart of the array, while 224 in the annular subpart (a roughly equal distribution on the base of the two different footprints is chosen). The layout of the non-optimized hybrid sparse array is the same depicted in the example of Fig. 2 (where the element center positioning is shown). The configuration reported in Fig. 2 with unitary element weights is used to initialize the optimization algorithm.

In Fig. 5 the layout of the optimized hybrid sparse array is depicted, while in Fig. 6 the related BPs (2D BP for a fixed φ angle compared with BP_d and the overall 3D BP) are shown. The obtained BP is similar to the desired BP over 360° of azimuth.

Then, the one-way and two-way BPs obtained with the non-optimized and the optimized hybrid sparse arrays are compared (broadside condition). The results of the beam profiles performed using Field II [6] are reported in Fig. 7. In the first figure (Fig. 7(a)), the 2D BPs of the transmitter dense array (unitary weights) for three fixed φ angles are reported. The BP is characterized by a main lobe width at -3 dB of 6.4°. In Figs. 7(b) and 7(c) the BPs of the non-optimized and the optimized receiver arrays are shown, while in Figs. 7(d) and 7(e) the relative two-way BPs are depicted. When the optimized array is used as receiver, a side lobe suppression is clearly visible in the two-way BP. The optimized array is characterized by a main lobe width at -3 dB of 2.4°, as imposed during the optimization process.

In Figs. 8 and 9 the 3D two-way BPs are shown when the broadside condition is assumed both for the transmission and the reception and when a steering of $\theta = 2°$ and $\varphi = 0°$ is considered for the reception in the case of non-optimized (Fig. 8) and optimized hybrid sparse arrays (Fig. 9), respectively. Furthermore, in the last case, the 3D two-way BP is reported when a steering of $\theta = 40°$ and $\varphi = 0°$ is considered both in transmission and reception.

The results clearly demonstrate a reduction of roughly 20 dB of the side lobe levels. Moreover, when the transmission and reception steering does not coincide, the undesired effect previously described is mainly removed.

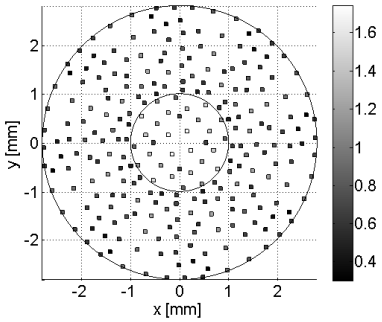

Fig. 5. Layout of the optimized hybrid sparse array.

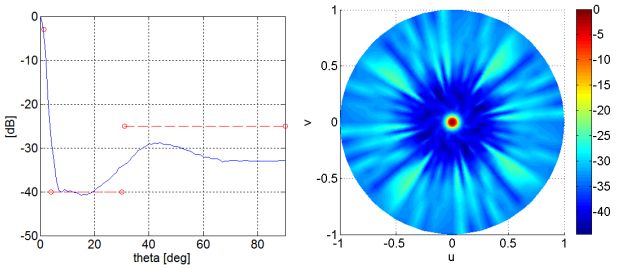

Fig. 6. 2D BP for a fixed φ angle ($\varphi = 45°$) compared with BP_d and the overall 3D BP of the optimized hybrid sparse array.

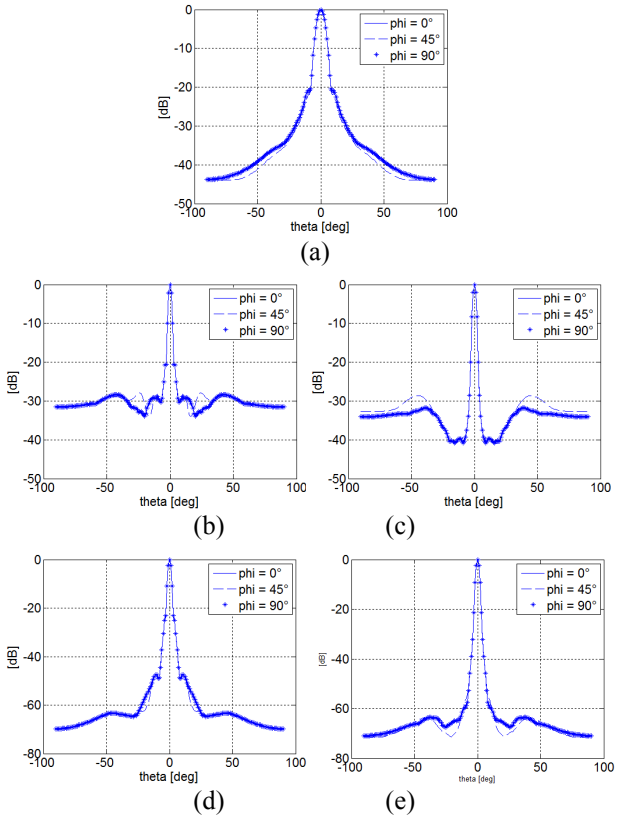

Fig. 7. 2D BP for fixed values of φ: $\varphi = [0°, 45°, 90°]$. (a) transmitter dense array; (b) non-optimized hybrid sparse array; (c) optimized hybrid sparse array; (d) two-way with non-optimized hybrid sparse array used in reception; (e) two-way with optimized hybrid sparse array used in reception.

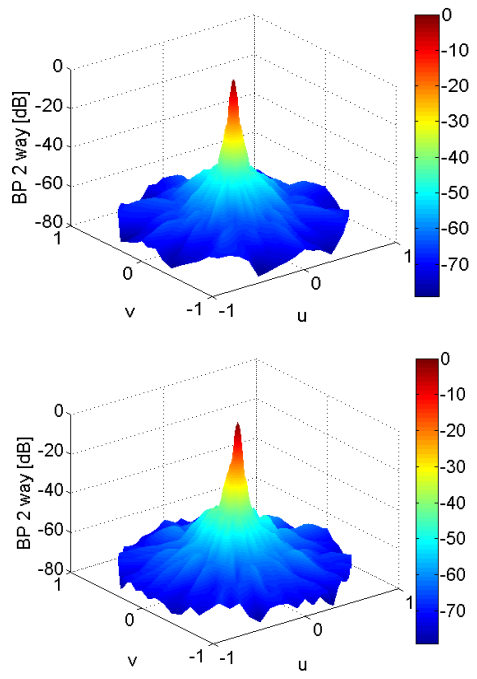

Fig. 8. 3D two-way BPs when the non-optimized hybrid sparse arrays is used in reception. Top: broadside; bottom: broadside transmission and steering of $\theta = 2°$ and $\varphi = 0°$in reception.

6. DISCUSSION

The results demonstrated that trough an opportune optimization of the receiver array it is possible to obtain a good lateral resolution (i.e., 1 mm) and to drastically reduce the side lobe levels in the two-way BP, especially when the transmission/reception steering directions do not coincide. This result is particularly important to validate the proposed transmission/reception strategy. Moreover, the obtained two-way BP is homogeneous over 360° of azimuth, since an opportune cost function have been introduced. Finally, we have verified that even for high elevation angles (i.e., 40 degree) a good performance in terms of acoustic beam characteristic, side lobes and grating lobes is maintained. Further improvements can be done by optimizing the number of elements that lays in the central and annular subparts of the receiver array. Moreover, the dimension and shape of the elements positioned in the annular subpart can be opportunely optimized.

7. CONCLUSIONS

An innovative transmission/reception solution, that involves a compact fully sampled 256-element circular array as transmitter and an optimized 256-element sparse array as receiver, referred to as hybrid sparse array, has been proposed. The solution is well-suited for real-time 3D imaging over 360° of azimuth and ±40° of inclination.

REFERENCES

[1] A. Trucco, "Thinning and weighting of large planar arrays by simulated annealing", *IEEE Transaction on Ultrasonics, Ferroelectrics and Frequency Control*, vol. 46, pp. 347-355, 1999.

[2] A. Trucco, "Weighting and thinning wide-band arrays by simulated annealing", *Ultrasonics*, vol. 40, pp. 485-489, 2002.

[3] A. Austeng and S. Holm, "Sparse 2-D arrays for 3-D phased array imaging – design methods", *IEEE Transaction on Ultrasonics, Ferroelectrics and Frequency Control*, vol. 49, pp. 1073-1086, 2002.

[4] B. Diarra, M. Robini, P. Tortoli, C. Chachard and H. Liebgott, "Design of optimal 2-D non-grid sparse arrays for medical ultrasound", *IEEE Transaction on Biomedical Engineering*, vol. 99, 2013.

[5] S. Kirkpatrick, C.D. Gellat and M.P. Vecchi, "Optimization by simulated annealing", *Science*, vol. 220, pp. 671-680, 1983.

[6] J.A. Jensen, "FIELD: A program for simulating ultrasound systems", *10th Nordic-Baltic Conference on Biomedical Imaging*, vol. 34, pp. 351-353, 1996.

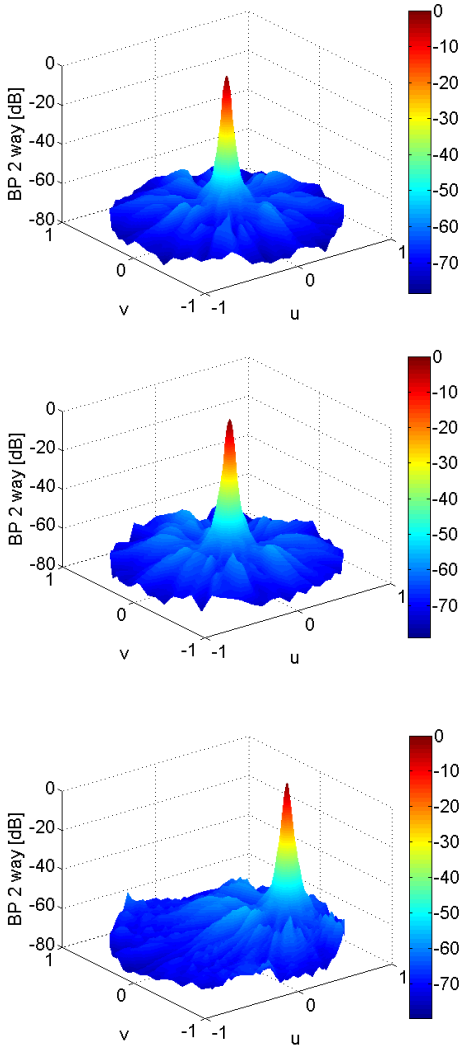

Fig. 9. 3D two-way BPs when the optimized hybrid sparse arrays is used in reception. Top: broadside; middle: broadside transmission and steering of $\theta = 2°$ and $\varphi = 0°$in reception; bottom: steering of $\theta = 40°$ and $\varphi = 0°$ in transmission and reception.